LETTER

Enhanced Catalytic Activity of Gold Nanoparticles Doped in a Mesoporous Organic Gel Based on Polymeric Phloroglucinol Carboxylic Acid–Formaldehyde

Han Yang,[†] Keiji Nagai,[*,‡] Toshiyuki Abe,[§] Hirofumi Homma,[†] Takayoshi Norimatsu,[†] and Ramasamy Ramaraj[†,||]

Institute of Laser Engineering, Osaka University, 2-6 Yamada-oka, Suita, Osaka 565-0871, Japan, Division of Integrated Molecular Engineering, Chemical Resources Laboratory, Tokyo Institute of Technology, R1-26, Nagatsuda 4259, Midori-ku, Yokohama 226-8503, Kanagawa, Japan, Department of Materials Science and Technology, Faculty of Science and Technology, Hirosaki University, 3 Bunkyo-cho, Hirosaki, Aomori 036-8561, Japan, and Centre for Photoelectrochemistry, Madurai Kamaraj University, Madurai 625 021, India

ABSTRACT Gold nanoparticles were supported by a phloroglucinolcarboxylic acid–formaldehyde (PF) gel, a new organic gel with a 30 nm spheroid-like structure. The surface area of the PF gel with gold nanoparticles was 550 m^2/g. Gold nanoparticles supported on a PF gel exhibited catalytic activity in the reduction of 4-nitrophenol with a reaction rate constant of 7.4×10^{-3} s^{-1}, which is high in the reported heterogeneous reaction system. The adsorption behavior of 4-nitrophenol into the gel support was observed by ultraviolet–visible absorption spectroscopy. Gold nanoparticles in the PF network were characterized by scanning electron microscopy, atomic force microscopy, and transmission electron microscopy observation. The high reduction rate would be attributed to the extraction and diffusion of the reactant through the pores of a PF gel support to encounter the highly dispersed gold nanoparticles on the surface and inside the material.

KEYWORDS: mesoporous support • organic gel • gold nanoparticles • catalysis • reduction • 4-nitrophenol

INTRODUCTION

Gold nanoparticles have received considerable attention because of their unique catalytic properties especially when dispersed on supports (1). Highly dispersed gold nanoparticles with diameters of less than 10 nm were highly active catalysts for some reactions (2–4), such as CO oxidation (5, 6) and NO reduction (7, 8). Parameters to control transition-metal heterogeneous catalysis include the particle composition, size and shape, support composition, and organizational structure of the supports. Porous materials (9–14) not only can maintain gold nanoparticles in a highly dispersed state because of their high surface areas (15) and porosity but also can work as absorbents of the reactants. The organizational structure of porous supports is composed of micropores ($d < 2$ nm), mesopores (2 nm $< d <$ 50 nm), and macropores ($d >$ 50 nm). Diffusion of the reactant occurs mainly in micropores, whereas meso- and macropores serve as passages to the micropores (15). The reactant molecules can diffuse through the pores to encounter the active nanoparticles, and the reaction occurs not only on the surface but also inside the material, which is advantageous for catalytic applications. Furthermore, the gel support not only can retard the sintering and increase the poison resistance of the active gold nanoparticles but also can avoid the contamination of products by the catalysts. Separation of the product from the catalyst particles could be done by filtration. In this study, a new organic gel, namely, phloroglucinolcarboxylic acid–formaldehyde (PF) (16, 17), instead of commonly used resorcinol–formaldehyde (RF) since the first introduction in 1989 (18), was chosen as the support of the gold nanoparticles because it provides a surface area twice as large as that of the RF gel (16, 17). Besides, the PF gel provides mesoporous structures of which the pore size is 30 nm on average (16, 17), while the pore size of the RF gel, which is mainly macropores, is 200 nm on average (19–22). Mesoporous structures can enhance the ability of this analogue of RF as an absorbent because of the capillary forces. The reactants can be absorbed in the pores of the PF gels at high concentration, which accelerates the catalytic reaction. The catalytic activity of the PF-gel-supported gold nanoparticles has been investigated by the reduction of 4-nitrophenol (4-NP) by sodium borohydride (23–28). Gold nanoparticles have usually been supported by polymers or resin beads. The porous structure of the PF gel was controlled by the gold nanoparticles in the about-to-gel (29) solution as reported for the RF

* To whom correspondence should be addressed. E-mail: nagai.k.ae@m.titech.ac.jp. Tel.: (+81) 45-924-5266. Fax: (+81) 45-924-5247.
Received for review June 30, 2009 and accepted August 28, 2009
† Osaka University.
‡ Tokyo Institute of Technology.
§ Hirosaki University.
|| Madurai Kamaraj University.
DOI: 10.1021/am900447c

Published on Web 09/04/2009

gel (19−22). The rate of the catalytic reaction in the presence of PF-gel-supported gold nanoparticles was compared with gold nanoparticles in other systems reported (23−28). The absorption behavior of the gel support was recorded by time-dependent ultraviolet−visible (UV−vis) absorption spectra.

EXPERIMENTAL SECTION

Gold Nanoparticles Colloidal Solution. A citrate-reduced gold nanoparticles colloidal solution was prepared by following the literature (30). A total of 1 mL of a 1 % $HAuCl_4$ solution was added to 90 mL of water at room temperature (20−23 °C). After 1 min of stirring, 2.0 mL of 38.8 mM sodium citrate was added. After 1 min, 1.0 mL of fresh 0.075 % $NaBH_4$ in 38.8 mM sodium citrate was added. The colloidal solution was stirred for an additional 5 min and stored in a dark bottle at 4 °C. The particle size was characterized by dynamic laser scattering nanoanalyzer (LB-550, Horiba, Japan).

Gold Nanoparticles Supported on PF Gels. Phloroglucinol-carboxylic acid (1.25 g; Tokyo Chemical Industry Co., Ltd., Tokyo, Japan) was dissolved into 22 mL of an alkaline water solution, which contained 5 mL of 1.0 M NaOH (Sigma Aldrich, Tokyo, Japan), and then 1.14 mL of a formaldehyde solution (37 %; Nacalai Tesque Inc., Kyoto, Japan) was immediately added. The mixture was stirred at 70 °C for 65 min, and the obtained PF solution was cooled down in an ice bath for 0.5 h. Then 1 mL of the gold colloidal solution, obtained by the above method, was added to the about-to-gel (29) PF solution. The amount of gold nanoparticles in the mixture was checked by inductively coupled plasma (ICP) spectrometry. The mixture was kept under room temperature for gelation. For a microstructure comparison, a PF gel without gold nanoparticles was obtained under the same conditions as those described above, except for the addition of 1 mL of pure water instead of a gold colloidal solution. PF gels with and without gold nanoparticles were extracted by a CO_2 supercritical fluid at 60 °C and 80 atm.

Transmission Electron Microscopy (TEM) Measurement for Gold-Nanoparticles-Doped PF Gels. TEM observation was conducted using a Hitachi H-8000 transmission electron microscope (accelerating voltage: 200 kV), in order to obtain a sample image and an electron diffraction pattern. For recording a TEM image, 0.01 cm^3 of the gold-nanoparticles-doped PF solution was dropped onto a microgrid supported on a copper grid mesh (Nisshin EM Co. Ltd., Tokyo, Japan) and dried at room temperature.

4-Nitrophenol (4-NP) Reduction. A mixture containing 2.7 mL of water and 0.15 mL of 1.0×10^{-3} M 4-NP was placed in a quartz cell. A gold-nanoparticles-doped PF gel, with a volume of 1.11×10^{-2} cm^3, was placed simultaneously into the cell. After absorption equilibrium was reached, 0.15 mL of 1.0×10^{-1} M $NaBH_4$ was added into the cell. The absorption spectra in the range of 200−800 nm were recorded every 90 s at room temperature by a Hitachi U-4100 spectrometer.

RESULTS AND DISCUSSION

The absorption spectrum of the fresh gold nanoparticles colloidal solution showed an additional absorption band at around 510 nm (Figure S1 in the Supporting Information). The gold nanoparticles were impregnated into the PF gel by adding the gold colloidal solution into the about-to-gel (29) PF solution. The UV−vis spectra of the PF gel film with and without gold nanoparticles are shown in Figure S2a in the Supporting Information. The absorption band of the PF gel film with gold nanoparticles shifts to a shorter wavelength, compared with that of the PF gel film without gold nanoparticles. After subtraction, the absorption spectrum showed the same band as that with gold nanoparticles (Figure S2b in the Supporting Information).

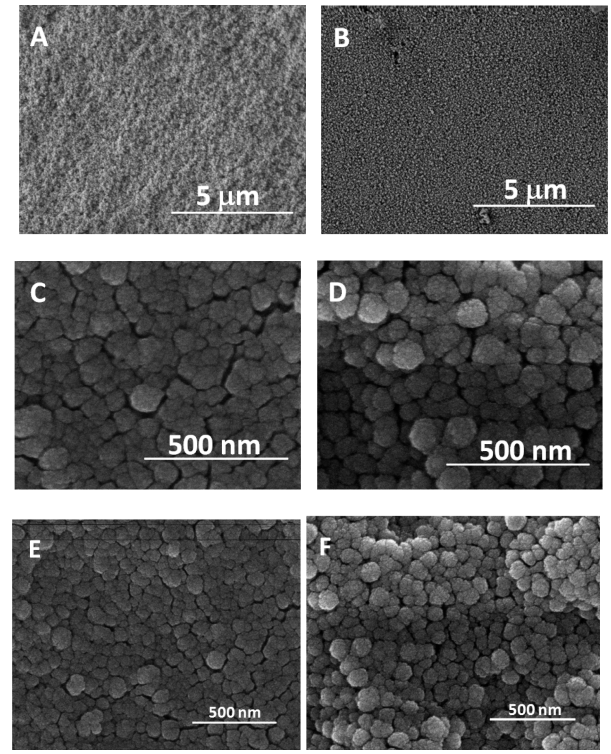

FIGURE 1. SEM images of the section parts of the PF aerogel films undoped with gold nanoparticles (A, C, and E) and doped with gold nanoparticles (B, D, and F). Images C and D were taken at high magnification.

The doping of gold nanoparticles affected the microporous structure of the PF gel according to the scanning electron microscopy (SEM) images of supercritical dried PF gels with and without gold nanoparticles. The SEM images in Figure 1 showed the morphologies of PF aerogels (PF gels after supercritical drying) without (Figure 1A,C) and with (Figure 1B,D) gold nanoparticles doping. Parts C and D of Figure 1 showed higher magnification images of parts A and B of Figure 1, respectively. The pore size of the PF aerogel was much smaller than that of the RF aerogel, and the pore size uniformity of the PF aerogel was better than that of the RF aerogel (16, 17), which would facilitate a high dispersion of gold nanoparticles. When the morphologies of the spheroids were compared at low magnification (Figure 1A,B), the spheroidlike structure of gold-nanoparticles-doped PF aerogel was more obvious, and each spheroid was more independent. The spheroids of gold-nanoparticles-doped PF aerogels showed clear three-dimensional spherical shapes and distinct boundaries, whereas the spheroids of undoped PF aerogels did not exhibit distinct boundaries. Some parts of the spheroids coagulated. Such a difference in the morphologies was more clearly shown at high magnification in Figure 1C−F. Spheroids of undoped PF aerogels exhibited smooth surfaces, whereas spheroids of the gold-nanoparticles-doped PF aerogel exhibited white dots on the surface of the spheroids. The atomic force microscopy (AFM) image in Figure S3a in the Supporting Information of the gold-nanoparticles-doped PF aerogel also exhibits bright dots of gold nanoparticles, while no such dots were observed in PF without gold nanoparticles (Figure S3b in the Supporting

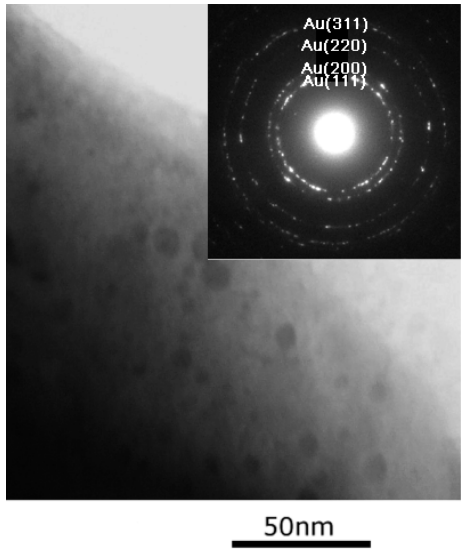

FIGURE 2. TEM image of the gold-nanoparticles-doped PF gel. The concentration of gold nanoparticles was 4×10^{-6} g/mL. The particle size was about 8 nm. Below is the electron diffraction pattern.

Information). These white dots were analyzed by the energy-dispersive X-ray spectrum (Figure S4 in the Supporting Information). The gold peak was observed at 9.72 keV (32). The size of the white dots on the surface was about 7 nm, which was consistent with the diameters of the gold nanoparticles obtained from a dynamic laser scattering particle analyzer (Figure S5 in the Supporting Information). The powder X-ray diffraction (XRD) pattern exhibited a broad reflection corresponding to the glass substrate. The sharp peaks can be indexed to the {111}, {200}, {220}, and {311} allowed reflecting planes expected from face-centered-cubic (fcc) gold. The average particle size was 8 nm for the peak of {111} estimated from the Scherrer equation (33). The TEM (Figure 2) image showed the gold nanoparticles on the surface of the PF spheroid. The particle size was about 8 nm, which was consistent with the SEM and XRD measurements. The characteristic rings in the polycrystalline diffraction pattern can be indexed to the {111}, {200}, {220}, and {311} allowed reflecting planes expected from fcc gold. The diffuse nature of the rings is a simple manifestation of the crystal shape effect due to the nanoscale size of the particles. Discrete gold particles were observed in electron micrographs, some of which exhibited characteristic {111} and {200} lattice fringes. The pore-size distribution of the gold-nanoparticles-doped PF gel was analyzed on the SEM image of Figure 1F. The size distribution of the pores against the line in Figure 1F is shown in Figure S7 in the Supporting Information, and the average pore size is about 11 ± 5 nm. From adsorption−desorption isotherms of N_2 (77 K) in Figure S8 in the Supporting Information, the Brunauer−Emmett−Teller surface area of an undoped PF aerogel was 490 m^2/g, whereas that of a gold-nanoparticles-doped PF aerogel was 550 m^2/g. The surface areas of both doped and undoped PF aerogels were twice as large as that of the RF aerogel (34). The isotherm exhibited a type IV N_2 sorption isotherm with a type H2 hysteresis loop (35) at a relative pressure (P/P_0) range from 0.7 to 0.95. This kind of isotherm and the hysteresis loop are attributed to capillary condensation in the mesopores (36), which would be useful for the PF gel as the absorbent of the reactant.

To study the catalytic activity of gold-nanoparticles-doped PF gels, the reduction of 4-NP by $NaBH_4$ was chosen as a model reaction. 4-NP is inert to $NaBH_4$ in the absence of gold nanoparticles. However, gold nanoparticles effectively catalyzed the reduction of 4-NP by acting as an electron relay system; electron transfer occurs between 4-NP and $NaBH_4$ through the gold nanoparticles. The kinetics of 4-NP reduction in the presence of PF-gel-supported gold nanoparticles was studied by UV−vis spectroscopy. The UV−vis spectra in Figure 3 showed the heterogeneous catalytic process of PF-gel-supported gold nanoparticles every 90 s. The concentration of gold nanoparticles was 4×10^{-6} g/mL, which was measured by ICP. The peak red-shifted from 317 nm (black line) to 400 nm (red line) because of the formation of 4-nitrophenolate ions in a $NaBH_4$ medium (pH > 12.0). The addition of a 0.1 cm^3 PF gel first caused the adsorption of 4-nitrophenolate ions and nearly simultaneously the reduction of 4-NP in the pores of PF where gold nanoparticles were presented.

$$NP_W \underset{k_{de}}{\overset{k_{ad}}{\rightleftharpoons}} NP_{PF} \tag{1}$$

$$\frac{d[NP_W]}{dt} = -k_{ad}[NP_W] + k_{de}[NP_{PF}] \tag{2}$$

The apparent adsorption rate constant (37) was determined by k_{ad} and k_{de}, as shown in eq 2. $[NP_{PF}]$ is the 4-nitrophenolate ion concentration inside the PF gel film, and $[NP_W]$ is the 4-nitrophenolate ion concentration in the solution outside the PF gel film. In order to calculate the apparent adsorption rate constant, the adsorption of the 4-nitropheniolate ion by blank PF gel films was studied by UV−vis spectroscopy. Figure S9a in the Supporting Information shows the UV−vis spectra of the 4-nitrophenolate ion solution with blank PF gel films. The absorbance at 400 nm of an outer solution decreased, which indicated the adsorption of the 4-nitrophenolate ion from outer solution by blank PF gel films. There was no further decrease when equilibrium was achieved. The Napierian logarithms of the absorbance of the 4-nitrophenolate ion in solution after adsorption ($\ln A$) were plotted against time (Figure S9b in the Supporting Information). A linear correlation with time was obtained for this adsorption system. The pseudo-first-order rate constant was 7.9×10^{-3} s^{-1} calculated from eq 3 in which ΔA_e is defined as the adsorption capacity at equilibrium and ΔA_t is defined as the adsorption amount at time t. The absorbance of the 4-nitrophenolate ion solution without blank PF gel films had no change over 30 min (Figure S9c in the Supporting Information).

$$\ln \frac{\Delta A_e}{\Delta A_e - \Delta A_t} = k_{ad} t \quad (3)$$

$$\frac{d[NP_{PF}]}{dt} = k_{ad}[NP_W] \quad (4)$$

From the calculation based on eq 4 and the law of Lambert−Beer, about 8×10^{-9} mol of 4-nitrophenolate ions was absorbed in the pores of the PF gel film with a pore volume of 8×10^{-2} cm^3. Therefore, the concentration of 4-nitrophenolate ions in the pores is about 1×10^{-4} M, which is as twice as the initial concentration of the outer 4-NP solution (5.0×10^{-5} M). The high concentration of reagent led to fast reduction.

For a reduction in the pores of the PF gel, because the concentration of sodium borohydride largely exceeds the concentration of 4-NP, the reduction rate can be assumed to be independent of the borohydride concentration. Therefore, pseudo-first-order rate kinetics with regard to the 4-nitrophenolate concentration could be used to evaluate the catalytic rate. The inset in Figure 3 shows the plot of ln A_1 (A_1 = absorbance at 400 nm; red marks) versus time. The red marks in the inset of Figure 3 show that the rate of decrease in the absorbance was constant at 7.4×10^{-3} s^{-1}, from which the pseudo-first-order rate was determined.

The RF gel, which has ~200 nm pore size (19−22), did not show adsorption of 4-NP, as shown in Figure S10a in the Supporting Information, so that the reduction of 4-NP did not happen in the presence of a gold-nanoparticles-doped PF gel (Figure S10b in the Supporting Information). This supports the theory that adsorption due to a mesoporous gel has an important role in inducing the high catalytic activity of the reduction. The reduction rate constant of the PF-gel-supported gold nanoparticles was compared with those of gold nanoparticles reported in different reaction systems, as listed in Table 1.

From Table 1, the reduction rate constant of the PF-gel-supported gold nanoparticles was the highest in the reported heterogeneous reaction system (23, 26). Compared with the homogeneous reaction system, the reduction rate constant of the PF-gel-supported gold nanoparticles was higher than that of nonsupported gold nanoparticles (24) and one of the dendrimer-supported gold nanoparticles (25). This high reduction rate was due to the high concentration of reagents as calculated above.

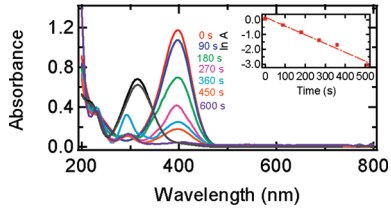

FIGURE 3. Successive UV−vis absorption spectra recorded at a time interval of 90 s. The black line is the absorption spectrum of 4-NP and a gold-doped PF gel without $NaBH_4$. The colored lines are the absorption spectra of the reduction of 4-NP by $NaBH_4$ in the presence of gold-nanoparticles-doped PF gel. In a $NaBH_4$ medium, the peak due to 4-NP (black line, λ_{max} = 317 nm) is red-shifted during the formation of the 4-nitrophenolate ion (λ_{max} = 400 nm). The peak of the 4-nitrophenolate ion vanished, and a new peak in the blue region gradually appeared because of the corresponding amino compound (λ_{max} = 290 nm). The inset is a plot indicating the variation of the Napierian logarithm of absorbance at 400 nm (red marks). Dashed lines are visual guides only.

Table 1. First-Order Rate Constant Calculated from ln *A* versus Time

sample	carrier system	metal	*D* (nm)	*k* (10^{-3} s^{-1})	*k*′ (10^{-2} s^{-1} m^{-2} L)
Au-PF	gel	gold	8	7.4	24.6[a]
Au-RF	gel	gold	8	0	0[b]
Au-PAMAM/PPI(25)	dendrimer	gold	8.3	1.78−13.2	17−126[a]
Au resin(23)	ion-exchange resin	gold	17	<1[c]	
Au(24)	None	gold	6.0	2.1	8.33[a]
Ag-PS-PEGMA(26)	Polymer brush	silver	7.5	0.335[c]	7.27

[a] k′ = k/S. The calculated data of rate constants normalized to the surface area *S*. The surface area was normalized to the unit volume of the system. [b] Figure S10 in the Supporting Information. [c] The calculated data of apparent rate constant in the literature.

The product of the amino compound was gradually released from the pores of the PF gel to the outer solution, as shown in eq 5. An additional peak at 290 nm, corresponding to the amino compound, was first observed at 90 s from the addition of $NaBH_4$ (Figure 3). Its absorbance increased slightly over 180 s. At 270 s, the absorbance of the peak at 290 nm increased significantly. This was because a large amount of the amino compound product was released to the solution after it became saturated in the pores of the PF gel.

$$AP_{PF} \underset{k_{ad}}{\overset{k_{de}}{\rightleftharpoons}} AP_W \quad (5)$$

$$\frac{d[AP_W]}{dt} = -k_{ad}[AP_W] + k_{de}[AP_{PF}] \quad (6)$$

During the whole process, there was no plasmon band of gold nanoparticles at 510 nm. This indicated that no gold nanoparticle clusters leached into the 4-NP solution. All of the catalyst material remained in the matrix of the PF gel. This is an efficient way to avoid contamination of the catalyst into the final product.

CONCLUSIONS

PF gel was used as the catalyst support. The porous PF-gel-supported gold nanoparticles showed catalytic activity in the reduction of 4-NP at a reaction rate of 7.4×10^{-3} s^{-1}, which is the highest in the reported heterogeneous reaction system. This would be attributed to the extraction and diffusion of reactants through the mesoporous PF gel support to encounter the highly dispersed gold nanoparticles on the surface and inside the material. The gold nanoparticles also

affected the microporous structure of the PF gel support. The gold-nanoparticles-doped PF gels exhibited an obvious spherical-like structure compared with undoped PF gels. The surface area changed from 490 m^2/g for an undoped PF aerogel to 550 m^2/g for a gold-nanoparticles-doped PF aerogel.

Acknowledgment. A part of this work was supported by a Grant-in-Aid for Scientific Research from MEXT Japan and a grant from the Japan Society for Promotion of Science. We are also thankful for technical support by K. Miyamoto.

Supporting Information Available: Spectra of gold nanoparticles, a blank PF gel, and a gold-nanoparticles-doped PF gel, AFM images of a blank PF aerogel and a gold-nanoparticles-doped PF aerogel, energy-dispersive X-ray spectrum of a gold-nanoparticles-doped PF aerogel, XRD spectra of gold nanoparticles, N_2 adsorption−desorption isotherms of a blank PF aerogel and a gold-nanoparticles-doped PF aerogel, and UV−vis spectra. This material is available free of charge via the Internet at http://pubs.acs.org.

REFERENCES AND NOTES

(1) Rodriguez, J. A.; Liu, G.; Jirsak, T.; Hrbek, J.; Chang, Z.; Dvorak, J.; Maiti, A. *J. Am. Chem. Soc.* **2002**, *124*, 5242–5250.
(2) Haruta, M. *CATTECH* **2002**, *6*, 102–115.
(3) Maduraiveeran, G.; Ramaraj, R. *Electrochem. Commun.* **2007**, *9*, 2051–2055.
(4) Thangavel, S.; Ramaraj, R. *J. Phys. Chem. C* **2008**, *112*, 19825–19830.
(5) Shi, F.; Zhang, Q. H.; Ma, Y. B.; He, Y. D.; Deng, Y. Q. *J. Am. Chem. Soc.* **2005**, *127*, 4182–4183.
(6) Lopez, N.; Nørskov, J. K. *J. Am. Chem. Soc.* **2002**, *124*, 11262–11263.
(7) Ueda, A.; Haruta, M. *Appl. Catal., B* **1998**, *18*, 115–121.
(8) Ueda, A.; Haruta, M. *Gold Bull.* **1999**, *32*, 3–11.
(9) Egger, C. C.; du Fresne, C.; Raman, V. I.; Schädler, V.; Frechen, T.; Roth, S. V.; Müller-Buschbaum, P. *Langmuir* **2008**, *24*, 5877–5887.
(10) Lukens, W. W.; Stucky, G. D. *Chem. Mater.* **2002**, *14*, 1665–1670.
(11) Horikawa, T.; Hayashi, J.; Muroyama, K. *Carbon* **2004**, *42*, 1625–1633.
(12) White, R. J.; Luque, R.; Budarin, V. L.; Clark, J. H.; Macquarrie, D. J. *Chem. Soc. Rev.* **2009**, *38*, 481–494.
(13) Warren, S. C.; Messina, L. C.; Slaughter, L. S.; Kamperman, M.; Zhou, Q.; Gruner, S. M.; DiSalvo, F. J.; Wiesner, U. *Science* **2008**, *320*, 1748–1752.
(14) Dandapat, A.; Jana, D.; De, G. *Adv. Mater. Interfaces* **2009**, *1*, 833–840.
(15) Rodeiquez-reinoso, F. *Carbon* **1998**, *36*, 159–175.
(16) Yang, H.; Nagai, K.; Nakai, M.; Norimatsu, T. *Laser Part. Beams* **2008**, *26*, 449–453.
(17) Ito, F.; Nagai, K.; Nakai, M.; Norimatsu, T.; Nikitenko, A.; Tolokonnikov, S.; Koresheva, E.; Fujimura, T.; Azechi, H.; Mima, K. *Jpn. J. Appl. Phys.* **2006**, *45*, L335–L338.
(18) Pekala, R. W. *J. Mater. Sci.* **1989**, *24*, 3221–3227.
(19) Bekyarova, E.; Kaneko, K. *Adv. Mater.* **2000**, *12*, 1625–1628.
(20) Maldonado-Hódar, F. J.; Pérez-Cadenas, A. F.; Moreno-Castilla, C. *Carbon* **2003**, *41*, 1291–1299.
(21) Nagai, K.; Azechi, H.; Ito, F.; Iwamoto, A.; Izawa, Y.; Johzaki, T.; Kodama, R.; Mima, K.; Mito, T.; Nakai, M.; Nemoto, N.; Norimatsu, T.; Ono, Y.; Shigemori, K.; Shiraga, H.; Tanaka, K. A. *Nucl. Fusion* **2005**, *45*, 1277–1283.
(22) Nikroo, A.; Czechowicz, D.; Paguio, R.; Greenwood, A. L.; Takagi, M. *Fusion Sci. Technol.* **2004**, *45*, 84–89.
(23) Praharaj, S.; Nath, S.; Ghosh, S. K.; Kundu, S.; Pal, T. *Langmuir* **2004**, *20*, 9889–9892.
(24) Rashid, M. H.; Bhattacharjee, R. R.; Kotal, A.; Mandal, T. K. *Langmuir* **2006**, *22*, 7141–7143.
(25) Hayakawa, K.; Yoshimura, T.; Esumi, K. *Langmuir* **2003**, *19*, 5517–5521.
(26) Lu, Y.; Mei, Y.; Walker, R.; Ballauff, M.; Drechsler, M. *Polymer* **2006**, 4985–4995.
(27) Lee, K. Y.; Hwang, J.; Lee, Y. W.; Kim, J.; Han, S. W. *J. Colloid Interface Sci.* **2007**, 476–481.
(28) Esumi, K.; Isono, R.; Yoshimura, T. *Langmuir* **2004**, *20*, 237–243.
(29) Morris, C. A.; Anderson, M. L.; Stround, R. M.; Merzbacher, C. I.; Rolison, D. R. *Science* **1999**, *284*, 622–624.
(30) Brown, K. R.; Walter, D. G.; Natan, M. J. *Chem. Mater.* **2000**, *12*, 306–313.
(31) Chirea, M.; Garc1á-Morales, V.; Manzanares, J. A.; Pereira, C.; Gulaboski, R.; Silva, F. *J. Phys. Chem. B* **2005**, *109*, 21808–21817.
(32) Andreescu, D.; Wanekaya, A. K.; Sadik, O. A.; Wang, J. *Langmuir* **2005**, *21*, 6891–6899.
(33) Wong, B.; Yoda, S.; Howdle, S. M. *J. Supercrit. Fluids* **2007**, *42*, 282–287.
(34) Ito, F.; Nagai, K.; Nakai, M.; Norimatsu, T. *Macromol. Chem. Phys.* **2005**, *206*, 2171–2176.
(35) Wang, X.; Liang, C.; Dai, S. *Langmuir* **2008**, *24*, 7500–7505.
(36) Lin, C.; Ritter, J. A. *Carbon* **1997**, *35*, 1271–1278.
(37) Dotzauer, D. M.; Dai, J.; Sun, L.; Bruening, M. L. *Nano Lett.* **2006**, *6*, 2268–2272.

AM900447C